Sensor signal processing

Frequency Estimation From Limited Samples: Nonlinearizing Time-of-Flight Radial Velocity Estimation

Lee Streeter[1]

[1] School of Engineering, University of Waikato, Hamilton 3216, New Zealand
[*] Member, IEEE

Manuscript received September 9, 2020; accepted September 27, 2020. Date of publication October 2, 2020; date of current version October 19, 2020.

Abstract—Radial motion in indirect time-of-flight range imaging causes instantaneous frequency shifts in the data. Instantaneous frequency estimation is a well studied topic, but existing methods are either computationally inefficient, or require a minimum of several tens of samples to be accurate. Time-of-flight range imaging satisfies neither of these conditions, necessitating a new technique. Through differentiation, a differential equation of the instantaneous frequency is derived, transformed to a nonstationary ordinary differential equation, and solved by polynomial solution. Hence, instantaneous frequency is recast as a linear algebraic inversion problem. Semisimulated experimental tests show the proposed method is accurate, with interquartile velocity precision of 1.5–6.3 m/s.

Index Terms—Sensor signal processing, doppler velocimetry, frequency estimation, signal processing, time-of-flight (ToF) ranging.

I. INTRODUCTION

The estimation of instantaneous frequency from sinusoidal data has broad applications, including in communications and ranging. This problem has drawn significant attention over many years, leading to fast solutions like autoregression based methods [1], [2] that require a substantial number of samples, to slower methods that work on limited samples, such as multiple signal classification (MUSIC) [3], [4]. Statistical estimators improve accuracy but, again, often at the cost of computation time and power [5]. Iterative schemes [5], [6] are also performant and flexible but, at the same costs as statistical techniques.

Time-of-flight (ToF) range imaging is a multiframe full-field imaging method, which is vulnerable to motion error but provides the opportunity to measure radial velocity as well [5], [7]. The very large scale integration of pixels into ToF image sensor arrays causes significant limitations on the number of samples per pixel that may be acquired, transmitted, and processed in the short amount of time required to obtain full-frame rate range imaging. Also, the sensors generate large volumes of data to process, creating the need for efficient frequency estimation methods on limited samples of one or two periods of harmonic data.

Previous work approaches the problem of motion in ToF imaging from an image processing perspective [8], [9], e.g., moving data within the frames so that a motion free range image is formed [10]. Hardware-based efforts tradeoff spatial resolution for temporal resolution, removing motion error at the cost of spatial blur [11], [12]. These techniques may be considered detect and fix approaches, which unfortunately discard data that may be useful, and moreover, misses the opportunity to measure the velocity of the motion itself.

In other previous work, radial velocity estimation computes a single pooled estimate over the raw frames, providing an estimate of linear velocity [5], [7]. The matrix pencil method has garnered attention in recent years in ToF (see, e.g., [11] and [13]), and much earlier in communications applications, e.g., [14]. The matrix pencil separates harmonic interference and multiple returns from the portion of the raw signal used to compute distance. This approach also provides pooled estimates of frequency (albeit, several), and not instantaneous frequency.

In this letter, we analyze the nonlinear radial velocity problem in ToF ranging, estimating instantaneous frequency estimation by transforming the data formation model into a regression problem.

II. THEORY

We take as a starting point the so-called correlation waveform representation of raw data, I_n, from a ToF camera [15]

$$I_n = \alpha \cos(\phi + \theta_n) + \beta \tag{1}$$

where ϕ is the range phase, which is linearly proportional to distance, α is the measured light return brightness, β is due to background light, and θ_n, $n \in \{0, \ldots, N-1\}$ are N programmed phase steps (often called phase shifts) typically evenly distributed between 0 and 2π. Radial motion causes ϕ to also depend on n. For convenience, we rewrite the abovementioned in continuous form $p(t) = \phi(t) + \theta(t)$ (and will return to the implications of sampling later), hence

$$I(t) = \alpha \cos(p(t)) + \beta. \tag{2}$$

Notice the implicit assumption that α and β remain constant.

The function $p(t)$ is the instantaneous phase of the correlation waveform. Consequently, the first time derivative, $\dot{p}(t)$, is the instantaneous frequency. In the context of ToF imaging, the instantaneous frequency is the instantaneous radial velocity. Differentiating $I(t)$ with respect to time gives

$$D_1(t) = \dot{I}(t) = -\alpha \sin(p(t))\, \dot{p}(t). \tag{3}$$

The instantaneous frequency is now exposed for estimation. Differentiating again results in

$$D_2(t) = \ddot{I}(t) = -\alpha \cos(p(t))\, \dot{p}^2(t) - \alpha \sin(p(t))\, \ddot{p}(t). \tag{4}$$

Letting $f(t) = \dot{p}(t)$, writing $\hat{I}(t) = \alpha \cos(p(t))$, and substituting $\hat{I}$ and $D_1(t)$ into $D_2(t)$, we obtain the following Bernoulli nonlinear differential equation for $f(t)$

$$D_1(t)\dot{f}(t) - D_2(t) f(t) = f(t)^3 \hat{I}. \tag{5}$$

Associate Editor: L. Azpilicueta.
Digital Object Identifier 10.1109/LSENS.2020.3028359

The usual strategy for solving Bernoulli equations is to perform the substitution $\gamma(t) = f^{-2}(t)$ (the power of -2 being specific to our case) which transforms (5) to the following nonstationary ordinary differential equation:

$$D_1(t)\dot{\gamma}(t) - 2D_2(t)\gamma(t) + 2\beta = 2\hat{I}(t) + 2\beta = 2I(t) \tag{6}$$

where we reintroduce β to account for the fact that we do not know it ahead of time and, hence, do not know $\hat{I}$.

$D_1(t)$ contains a sine function, which has zeros, rendering closed form solutions like integration by parts unstable, and likewise for classical numerical techniques such as Euler's method (and its extensions). We investigate solving (6) by polynomial. To such end, let $\gamma(t) = \sum_{m=0}^{M} a_m \theta(t)^m$, where M is a nominated polynomial order. Substituting into (6)

$$D_1(t)\sum_{m=1}^{M} m a_m \theta(t)^{m-1} - 2D_2(t)\sum_{m=0}^{M} a_m \theta(t)^m + 2\beta = 2I(t) \tag{7}$$

rearranging

$$\sum_{m=1}^{M} \left(D_1(t) m\theta(t)^{m-1} - 2D_2(t)\theta(t)^m\right) a_m - 2a_0 D_2(t) + 2\beta = 2I(t) \tag{8}$$

and factorizing using vector dot product multiplication gives

$$\left[M D_1(t)\theta(t)^{M-1} - 2D_2(t)\theta(t)^M, \ldots, -2D_2(t), 1\right] \cdot [a_M, \ldots, a_0, 2\beta] = 2I(t). \tag{9}$$

III. METHODS

Returning now to the discrete formulation

$$I_n = \alpha\cos(p_n) + \beta \tag{10}$$

the $D_1(t)$ and $D_2(t)$ are approximated by the numerical differences

$$D_{1n} = \frac{\alpha\cos(p_{n+1}) - \alpha\cos(p_n)}{\Delta\theta} = -\frac{\alpha\sin(\bar{p}_n)s_n}{\Delta\theta} \tag{11}$$

where $\Delta\theta$ is the step size, $\bar{p}_n = (p_{n+1} + p_n)/2$ and $s_n = \sin(\Delta p_n/2)$, and

$$D_{2n} = \frac{-2\alpha\sin(\bar{p}_{n+1})s_{n+1} + 2\alpha\sin(\bar{p}_n)s_n}{\Delta\theta^2}. \tag{12}$$

Writing $s_{n+1} = s_n + \Delta s_n$, D_{2n} reduces to

$$D_{2n} = -\frac{4\alpha\cos\left(\bar{\bar{p}}_n\right)s_n\bar{s}_n - 2\alpha\sin(\bar{p}_{n+1})\Delta s_n}{\Delta\theta^2} \tag{13}$$

where $\bar{s}_n = \sin(\Delta\bar{p}_n/2)$, echoing the form of (4). Assuming that Δp_n is small, then $s_n \approx \Delta p_n/2$, and

$$D_{2n} \approx \frac{\alpha\cos\left(\bar{\bar{p}}_n\right)\Delta p_n^2 - \alpha\sin(\bar{p}_{n+1})\Delta^2 p_n}{\Delta\theta^2}. \tag{14}$$

Therefore, by sampling $\theta(t)$, hence $\gamma(t)$, at N discrete steps, (9) becomes

$$\left[M D_{1n}\theta_n^{M-1} - 2D_{2n}\theta_n^M, \ldots, -2D_{2n}, 1\right] \cdot [a_M, \ldots, a_0, 2\beta] \approx 2I_n. \tag{15}$$

If $N \geq M + 2$, then (15) may be written as a fully determined matrix equation, and the a_m (and β) computed in closed form by linear regression. Once solved, γ_n is reconstructed, and $f_n = \Delta p_n$ computed.

Let X_M be the matrix with rows $[\theta_n^M, \ldots, \theta_n^0, 1]$, X_{M-1} be the matrix with rows $[M\theta_n^{M-1}, \ldots, \theta_n^0, 0, 0]$, D_1 be the diagonal matrix with nth diagonal entry D_{1n}, and likewise, D_2 be the diagonal matrix with diagonal entry D_{2n} and the vector involving the a_n and 2β as $\mathbf{a}$. Equation (15) may be rewritten

$$A\mathbf{a} \approx 2\mathbf{I} \tag{16}$$

where $A = (D_1 X_{M-1} - 2D_2 X_M)$, and $\mathbf{I}$ is the vector with nth entry I_n. Assuming $\mathbf{I}$ has noise with variance σ^2, and A is left invertible, then the noise in the estimate of $\mathbf{a}$ behaves as [16], [17]

$$\sigma_{\mathbf{a}}^2 \approx \frac{\sigma^2}{N}\mathrm{Tr}\left(\left(A^T A\right)^{-1}\right)(1 + 8M) \tag{17}$$

where $\mathrm{Tr}(\cdot)$ is the matrix trace, and $\cdot^T$ is the matrix transpose. For small α, $N \leq 12$, and $\alpha/\sigma > 10$, (17) may be further approximated by

$$\sigma_{\mathbf{a}}^2 \approx \frac{\sigma^2}{2\alpha^2 N}\mathrm{Tr}\left(\left(X_M^T X_M\right)^{-1}\right)(1 + 8M). \tag{18}$$

The uncertainty in f may then be found by propagation of uncertainty formulae [18].

It must be acknowledged that the approximations in (14) cause biasing error in estimating f_n. The error in $s_n \approx \Delta p/2$ reaches, e.g., 4% at $\Delta p = 0.99$ rad (2 s.f.), biasing the estimate. The sine term in D_{2n} appears exactly in D_{1n} (hence is not, in fact, an approximation). In the special case of constant velocity, the "graph" of p_n with θ_n is a straight line, and therefore, the further approximation $\cos(\bar{\bar{p}}_n) \approx \cos(p_n)$ becomes an exact equality. Error incurs with second and, more rapidly with, third-order motion, however, and the exact error is dependent on p_n. We test the least squares polynomial fitting nonlinear radial velocity estimation described earlier by simulation. The number of phase steps is varied from 5 to 12, and evenly stepped over both 2π and 4π radians. The phase function p_n is simulated as a third-order polynomial

$$p_n = \phi_0 + c_1\theta_n + c_2\theta_n^2 + c_3\theta_n^3 \tag{19}$$

with coefficients $c_1, \ldots, c_3$ that are varied independently of each other. Polynomial orders of $M = 1$ and $M = 2$ are both tested. In the simulations $\alpha = 1$ and $\beta = 2$. For each velocity simulation, 100 trials are performed where the initial phase ϕ_0 is randomly set for each trial and Gaussian random noise of standard deviation $\sigma = 0.01$ is added to the I_n. Using error propagation formulae [18], the random noise in classical ranging has standard deviation $\sigma_\phi = \sqrt{2}\sigma/\alpha \approx 0.014$ radians (ignoring motion error bias) serving as a baseline for error in estimates to follow. The root-mean-squared error is taken over the $N - 1$ phase steps pooled over the one hundred trials ($100(N - 1)$ data for each RMSE value, $N - 1$ due to taking the numerical derivative of p_n). We also perform a semisimulated test using real data from a proprietary prototype ToF camera running with modulation frequency 70 MHz. The camera is set to take nine raw frames per set at raw frame rate 270 FPS (comprising 30 range images per second in the traditional ToF imaging mode). A white foam board target was fixed to a 3.4 m Macron6 translation stage (Macron Dynamics, Croydon, PA) and moved from 1 to 3.4 m from the camera in 5 mm increments. Radial motion profiles are generated with random start position, initial velocity in the range -30–30 m/s, acceleration in the range -10–10 m/s^2, and jerk from -5–5 m/s^3. The motion profiles are generated and tested repeatedly until we obtain 10 000 sets starting and ending within the position range. For each profile, a pixel is selected at random on the target object, and at each simulated time step, the data for the nearest position was extracted from the corresponding phase step. We compute the estimated velocity between raw frames (as distance times frame per second), plotting the pooled estimated velocity over all trials against the true velocity. The change in distance per raw frame period

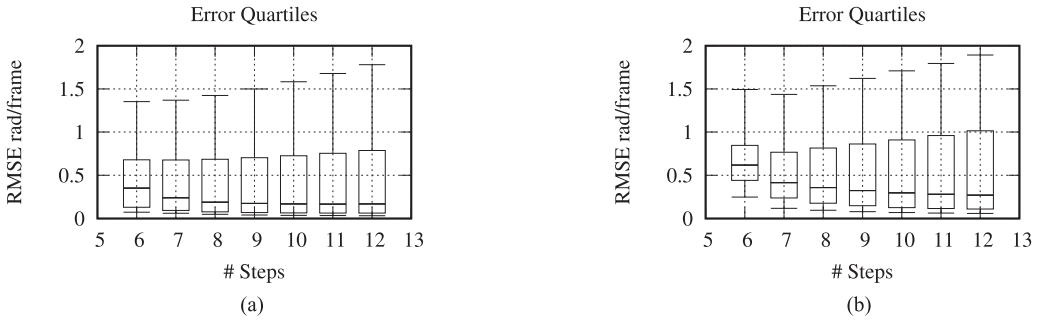

Fig. 1. Comparison of the estimation of instantaneous frequency using first- and second-order polynomials from samples of the correlation waveform spread over 2π. The error using a first-order polynomial is lower than that of using the second order, but overall, the error is unacceptably high. (a) First-order estimation of γ. (b) Second-order estimation of γ.

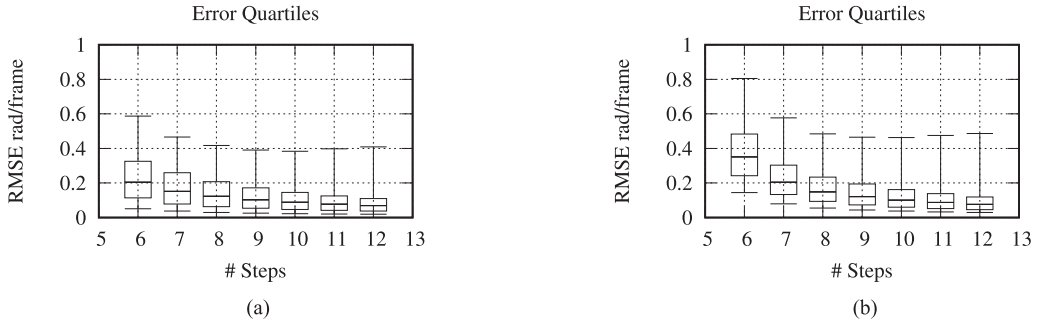

Fig. 2. Error in estimating frequency using first- and second-order polynomials from correlation waveform samples spread over 4π. Spreading the samples over the larger range assures sampling over more than one period, improving estimation. (a) First-order estimation of γ. (b) Second-order estimation of γ.

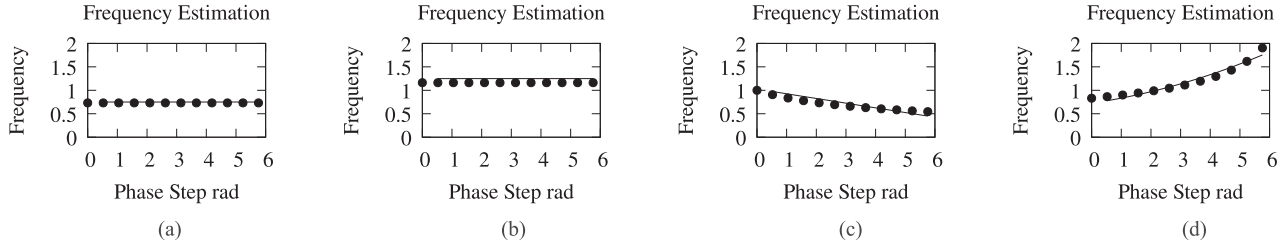

Fig. 3. Simulated velocity estimation. The solid line is the true radial velocity and the dots represent the estimates by the proposed method. (a) Linear velocity toward the camera. (b) Linear velocity away from the camera. Approximation error affects the estimation. (c) Acceleration toward the camera. (d) Initial velocity toward the camera, with acceleration and jerk away from the camera.

is calculated as

$$\frac{\Delta d_n}{\Delta t} = 30N \frac{c}{2\pi f_{\text{mod}}} (f_n - 1) + C \tag{20}$$

where 30 is the target range frame rate of the camera, f_{mod} is the camera modulation frequency [15], c is the speed of light in a vacuum, and as noted in earlier work [5], [7], harmonic interference causes bias in the velocity prediction, which we inspect and correct via the constant C.

IV. RESULTS AND DISCUSSION

In the simulation tests with samples over 2π, Fig. 1, the error is unacceptably large. The compression of the correlation waveform by motion toward the camera causes the samples to span less than one full period, providing inadequate information for recovering the instantaneous frequency. Sampling over 4π on the other hand reduces the error dramatically, seen in Fig. 2 (note the reduced y-axis range versus Fig. 1) with a trend of decreasing error with the number of phase steps, in accordance with the abovementioned discussion on approximation error. The error in Fig. 2 is still quite large, but one must bear in mind that the spread of motion parameters tested in simulation is also very large, simulating motion beyond what we would ordinarily require a ToF camera to measure. It is apparent that using second-order estimation of γ offers no clear advantage over first order; therefore, we use first-order estimation in subsequent tests.

Some specific simulation examples of simulated estimation of instantaneous frequency are given in Fig. 3, again over 4π. Constant motion toward the camera [see Fig. 3(a)], provides adequately dense sampling that, coupled with the extended range, the approximation error is small, and the estimated points follow the true frequency closely. For the motion away from the camera, the reduced sampling density causes the bias seen in Fig. 3(b). However, in both cases, the proposed

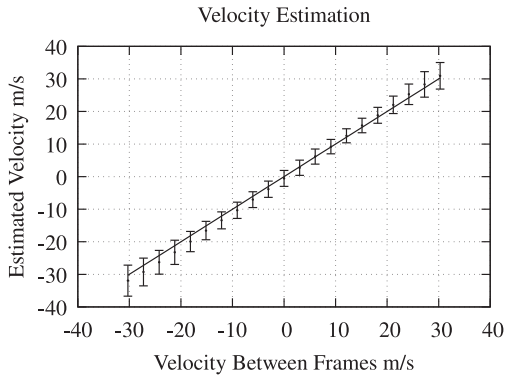

Fig. 4. Estimation of velocity with nonlinear motion, simulated but with real range imaging camera raw frame data. The velocities represented in the graph are between the pairs of raw frames. Dots represent means and the error bars are one standard deviation.

method predicts constant instantaneous frequency. Increasing the order of the motion in Fig. 3(c) and (d), we see phase step dependence in the error, but encouragingly, the estimates follow the reference lines.

We show the semisimulated test on real camera data in Fig. 4. Based on the results in Fig. 2, we choose $N = 9$ phase steps spread over 4π radians. By inspection we find the correction factor $C = 14$ m/s. We present the comparison of estimated velocity with true velocity between raw frames in Fig. 4, where the error bars represent the 25 and 75% quartiles. The interquartile widths range from 1.5 to 6.3 m/s. The smaller motion has minimal difference in distance between raw frames, causing the least change in raw frame pixel brightness; therefore, the numerical differences have the smallest error at small motion. The result in Fig. 4 demonstrates the success of the proposed instantaneous velocity estimation, but also that it is strongest at low speeds and that error increases with velocity. The standard deviation is smaller than the earlier attempts at linear velocity estimation [5], but larger than the more recent results [7] wherein standard deviations better than 1 m/s were achieved. In that earlier work, however, an average radial velocity was found over the whole phase step set, in contrast here we resolve down to each raw frame.

The primary advantage of the proposed method is the estimation of instantaneous frequency. The efficiency is $O((M+2)^3)$, which is approximately the same as MUSIC, but MUSIC requires a number of such operations to perform eigenvector analysis, whereas the method proposed herein only requires one. Moreover, MUSIC cannot time resolve the estimates. The matrix pencil likewise calls for eigenvector analysis. The linear velocity estimation [7] is asymptotically $O(N)$. Autoregression requires more samples than what we have tested here and cannot be directly compared.

V. CONCLUSION

In summary, we have demonstrated instantaneous frequency measurement from samples over about two wave periods in the context of radial velocity measurement in ToF range imaging. Analysis of the so-called correlation waveform that emerges from each pixel of a ToF ranging camera transformed the problem to a Bernoulli differential equation, which was linearized and solved by polynomial and linear regression. While approximations made in the numerical solution introduced 3(c) and (d), we see phase bias, tests demonstrated the success of the proposed method. A final linear calibration was required to convert from instantaneous frequency to radial velocity, and in future work, we will investigate in detail the impact of harmonic interference.

ACKNOWLEDGMENT

This work was supported in part by the Royal Society of New Zealand Marsden Council Fast Start under Grant UOW1501 and in part by the New Zealand Ministry of Business, Innovation and Employment Smart Ideas (UOWX1705).

REFERENCES

[1] P. Stoica and R. Moses, *Spectral Analysis of Signals*. Englewood Cliffs, NJ, USA: Prentice-Hall, 2005.
[2] Pierre Brémaud, *Fourier Analysis and Stochastic Processes*. Berlin, Germany: Springer, 2014.
[3] R. Whyte, L. Streeter, M. J. Cree, and A. A. Dorrington, "Application of lidar techniques to time-of-flight range imaging," *Appl. Opt.*, vol. 54, no. 33, pp. 9654–9664, Nov. 2015.
[4] A. Kadambi, J. Schiel, and R. Raskar, "Macroscopic interferometry: Rethinking depth estimation with frequency-domain time-of-flight," in *Proc. IEEE Conf. Comput. Vis. Pattern Recognit.*, Seattle, WA, USA, 2016, pp. 893–902.
[5] L. Streeter, "Stochastic calculus analysis of optical time-of-flight range imaging and estimation of radial motion," *J. Opt. Soc. Am. A*, vol. 34, no. 7, pp. 1063–1072, 2017.
[6] K. Mahata and M. M. Hyder, "Fast frequency estimation with prior information," *IEEE Trans. Signal Process.*, vol. 66, no. 1, pp. 264–273, Jan. 2018.
[7] L. Streeter, "Methods for linear radial motion estimation in time-of-flight range imaging," *Proc. SPIE*, vol. 10332, 2017, Art. no. 103320C.
[8] S. Lee, "Time-of-flight depth camera motion blur detection and deblurring," *IEEE Signal Process. Lett.*, vol. 21, no. 6, pp. 663–666, Jun. 2014.
[9] D. Jimenez, D. Pizarro, and M. Mazo, "Single frame correction of motion artifacts in PMD-based time of flight cameras," *Image Vis. Comput.*, vol. 32, no. 12, pp. 1127–1143, 2014.
[10] L. Streeter and A. A. Dorrington, "Coded exposure correction of transverse motion in full-field range imaging," *Opt. Eng.*, vol. 53, no. 10, 2014, Art. no. 102109.
[11] M. H. Conde, K. Kagawa, T. Kokado, S. Kawahito, and O. Loffeld, "Single-shot real-time multiple-path time-of-flight depth imaging for multi-aperture and macro-pixel sensors," in *Proc. IEEE Int. Conf. Acoust., Speech Signal Process.*, Barcelona, Spain, 2020, pp. 1469–1473.
[12] D. Kim *et al.*, "A dynamic pseudo 4-tap CMOS time-of-flight image sensor with motion artifact suppression and background light cancelling over 120klux," in *Proc. IEEE Int. Solid-State Circuits Conf.*, San Francisco, CA, USA, 2020, pp. 100–102.
[13] A. Bhandari, M. Feigin, S. Izadi, C. Rhemann, M. Schmidt, and R. Raskar, "Resolving multipath interference in Kinect: An inverse problem approach," in *Proc. IEEE SENSORS*, Valencia, Spain, 2014, pp. 614–617.
[14] N. Dharamdial, R. Adve, and R. Farha, "Multipath delay estimations using matrix pencil," in *Proc. IEEE Wireless Commun. Netw.*, 2003, vol. 1, pp. 632–635.
[15] D. Lefloch *et al.*, *Technical Foundation and Calibration Methods for Time-of-Flight Cameras*. Berlin Germany: Springer, 2013, pp. 3–24.
[16] G. W. Stewart, "Stochastic perturbation theory," *SIAM Rev.*, vol. 32, no. 4, pp. 579–610, 1990.
[17] N. Moriya, "On high-order discrete derivatives of stochastic variables," *Appl. Math. Model.*, vol. 30, no. 9, pp. 816–823, 2006.
[18] Evaluation of Measurement Data—Guide to the Expression of Uncertainty in Measurement (GUM), 2008.